



1 **Persistent warming of the ground on the Earth's Third Pole**

2 Yuyang Wang<sup>1</sup>, Jinzhi Ding<sup>2\*</sup>, Shilong Piao<sup>1,2</sup>

3 <sup>1</sup>Sino-French Institute for Earth System Science, College of Urban and Environmental Sciences,

4 Peking University, Beijing 100871, China

5 <sup>2</sup>State Key Laboratory of Tibetan Plateau Earth System, Resources and Environment (TPESRE),

6 Institute of Tibetan Plateau Research, Chinese Academy of Sciences, Beijing 100101, China

7

8 To whom correspondence may be addressed:

9 Prof. Dr. Jinzhi Ding, [jzding@itpcas.ac.cn](mailto:jzding@itpcas.ac.cn)

10

11

12

13

14

15

16

17

18

19



20 **Abstract**

21 A continuously increasing ground temperature in the Tibetan Plateau (TP) can result in permafrost  
22 degradation and impact regional climate through land-atmosphere interactions. However, systematic  
23 knowledge of spatiotemporal dynamics and regulatory mechanisms of ground temperature changes in  
24 the region is limited. Here, we quantify the thermal status and trends of both soil temperatures  
25 measured at depth and typical permafrost profile temperatures. We show that, shallow soil layers (0-40  
26 cm) in most TP regions experienced significant warming from 1981 to 2021, with lower rates at greater  
27 depths. Ground surface warming trends aligned with air temperature, but the timing of the maximum  
28 warming trend was progressively delayed with depth. Cold seasons exhibited the largest warming  
29 trends for air and ground surface, while warm seasons saw greater warming trends at 5-40 cm soil  
30 depths. Regionally, warming trends were larger at sites with lower mean annual temperature and higher  
31 elevation. Out of the factors tested in addition to air temperature, only snow-cover days and downward  
32 longwave radiation were significantly related to the soil warming rate trends. Further analysis reveals  
33 that the persistent shallow ground temperature increase over decades is linked to the Atlantic  
34 Multidecadal Oscillation's warm phase, impacting near-surface air temperature through teleconnections.  
35 Additionally, we present spatially heterogeneous observations of continuous warming in permafrost  
36 profiles, which show intense warming in the surface layers, and minimal warming at 40 m depth.  
37 Permafrost profile warming magnitude and depth-dependent variation are influenced by local climate  
38 and elevation. This study provides a comprehensive view of persistent warming in the Tibetan Plateau  
39 across surface and deep layers.

40 **Keywords:** Persistent warming, surface soil temperature, frozen ground region, Tibetan Plateau



41 **1. Introduction**

42 The thermal regime of the ground is a critical factor regulating interactions and feedbacks among  
43 multi-sphere systems in cold regions (Biskaborn et al., 2019; Smith et al., 2022). One of the  
44 fundamental parameters of the land's thermal regime is soil temperature which plays an essential role  
45 in land-atmosphere interactions and has significant effects on the climate (Zhang et al., 2021).  
46 Increased greenhouse gas emissions caused by human activities have resulted in continuous and rapid  
47 global atmospheric warming, leading to near-surface air warming and persistent warming of both the  
48 active layer and the deeper permafrost layer through downward heat transfer (IPCC, 2021). Changes in  
49 soil temperature involve both above-ground and below-ground processes, meaning that soil warming  
50 influences for example, energy and water cycles, biogeochemical processes, infrastructure stability  
51 (Chen et al., 2021c; Hjort et al., 2022; Wang et al., 2023). However, understanding the spatiotemporal  
52 dynamics and regulatory mechanisms of soil temperature changes is challenging for many reasons,  
53 including limited and unevenly distributed observation sites, high levels of spatial heterogeneity, and an  
54 oversimplified representation of complicated soil thermal transfer processes in current models (Chen et  
55 al., 2021a; Etzelmüller et al., 2020; Qian et al., 2011).

56 Previous studies have demonstrated that air temperature largely controls variations in the ground  
57 temperature at shallow depths (Melo-Aguilar et al., 2022; Petersen, 2021; Qian et al., 2011; Wang et al.,  
58 2018). However, the coupling between air and shallow ground temperatures is strongly influenced by  
59 buffer zones, such as vegetation, snow cover, and organic layers (Smith et al., 2022). Ground  
60 temperature fluctuations decrease with depth and respond with a lag to surface air temperature due to  
61 the filtering effect of the ground on high-frequency variations (Chen et al., 2021a; Smith et al., 2022).  
62 Ground- warming drivers and air-ground temperature coupling exhibit complex spatial, temporal, and



63 vertical variability, with different factors dominating in different regions. For example, Qian et al (2011)  
64 attributed soil warming in Canada from 1958 to 2008 mainly to trends in air temperature and snow-  
65 cover depth, while Chen et al (2021b) suggested that snow-cover thickness was the primary factor  
66 controlling trends in the difference between air and soil temperatures over Northern Eurasia, followed  
67 by snow-cover duration and solar radiation. Studies of the thermal regime deep underground (several  
68 dozen meters) have mainly been conducted in the permafrost region of the circumpolar Arctic and the  
69 Tibetan Plateau (Biskaborn et al., 2019; Cao et al., 2018; Etzelmüller et al., 2020; Zhao et al., 2010).  
70 Etzelmüller et al (2020) analyzed permafrost dynamics in European mountains and found that, during  
71 the past 20 years, deep permafrost had warmed at all the sites studied, with warming rates tending to be  
72 smaller in warm permafrost, due to latent heat effects. Additionally, various factors such as regional  
73 climate, elevation, topography, soil water and ice content, lithology, and geological structure may also  
74 affect changes in ground temperature. An integrated analysis of these complex factors is required to  
75 understand the spatiotemporal dynamics and regulatory mechanisms of ground temperature changes.  
76 Such understanding is crucial for predicting the impact of climate change on ecosystems and human  
77 activities.

78 The Tibetan Plateau (TP), known as the Earth's Third Pole, has the world's largest permafrost zone  
79 outside of the polar regions (Zou et al., 2017). It has been suggested that this Tibetan permafrost is  
80 distinct from circumarctic permafrost in that it is more vulnerable to climate change due to higher  
81 temperatures, lower ice content, thicker active layers, and thinner permafrost layers (Wang et al., 2022).  
82 The plateau's frigid climate has led to a significant organic carbon buildup in the soil (Ding et al., 2016).  
83 Observations have revealed that over the past 50 years the plateau has experienced significant warming,  
84 twice as fast as the global average, with a corresponding rise in the frequency of extreme temperatures



85 including heatwaves. This amplified warming has resulted in a substantial increase in ground  
86 temperature and an accelerated release of soil organic carbon from the TP, exacerbating the positive  
87 feedback between carbon release and climate warming (Taihua et al., 2020; Yang et al., 2019; Zhao et  
88 al., 2020). Additionally, continual increases in surface temperature may have a significant impact on  
89 regional (and larger-scale) climate change through land-atmosphere interactions (Yao et al., 2019). To  
90 gain better insight into the thermal status of the ground and regional changes across the Earth's Third  
91 Pole, it is crucial to understand the spatio-temporal dynamics and regulatory mechanisms of layered  
92 soil and deep ground warming.

93 This study aims to provide a comprehensive understanding of the implications of recent variations  
94 in ground temperature across the Tibetan permafrost regions. We analyzed ground temperature  
95 measurements made at various depths over the past several decades. These data were obtained from  
96 both meteorological observation sites and permafrost borehole sites. Specifically, our analysis focuses  
97 on temporal trends and the spatial distribution characteristics of layered ground temperature changes,  
98 including the active layer and the permafrost layer, at annual and interannual scales from 1981 to 2021.  
99 Additionally, we investigate the driving mechanisms behind ground temperature variations on the TP.

## 100 **2. Data and methods**

### 101 **2.1. Data compilation**

102 The ground temperature observation networks primarily cover the central and eastern regions of  
103 the TP, where there is considerable variation in climate due to altitude and geographic position (Fig. 1).  
104 The daily soil temperature data were collected from meteorological observation stations operated by  
105 the China Meteorological Administration (<http://www.nmic.gov.cn>). These data consist of mean soil



106 temperatures measured at the ground surface (0cm) and at seven depths below the surface: the shallow  
107 measurements at 5, 10, 20 and 40 cm, and the deeper ones at 80, 160 and 320 cm. To monitor ground  
108 surface (0 cm) temperature, surface geothermometers were placed on bare ground (Wang et al., 2018).  
109 Prior to 2005, during the winter snowfall, the snow surface temperature was used as the 0 cm soil  
110 temperature measurement, while after 2005, the ground surface temperature beneath the snow was used.  
111 Shallow soil temperatures (5-20 cm) were measured with curved tube thermometers, while deep soil  
112 temperatures (40-320 cm) were measured with straight tube thermometers (Shi et al., 2021). Due to the  
113 harsh environment of the TP, there were frequent instrument failures during the early years of soil  
114 temperature observations, and so we selected a time series for analysis from January 1st 1981 to  
115 February 28th 2022 which had relatively little missing data. However, because of a restriction imposed  
116 by data sharing policies, the 80 to 320 cm soil temperature time series began in 2007. Some missing  
117 data are inevitable for most long-term soil temperature monitoring sites due to harsh conditions or  
118 instrument malfunctions, and we therefore conducted strict quality control assessments of the soil  
119 temperature observations from all the available sites and selected data from high-quality and long-term  
120 sites for this analysis (Wang et al., 2018). The number of sites with shallow soil data (0-40 cm)  
121 available for analysis decreases with increasing measurement depth, however.

122 We also extracted daily air temperature, precipitation and snow depth data from the  
123 meteorological observation station records to investigate the potential influence of environmental  
124 factors on soil temperature variations. These daily observations were averaged or summed into monthly  
125 or annual values: mean annual air temperature (MAAT), mean annual soil temperature (MAST), annual  
126 rainfall (PPT), snow-cover days (SCD, the total number of days with snow cover) and the annual mean  
127 of daily snow depth. In addition to these *in-situ* observations, ERA5-Land monthly averaged products



128 from 1981-2021, including volumetric water content (SWC), surface net solar radiation and surface  
129 downwards thermal radiation (DLR), were accessed at <https://cds.climate.copernicus.eu/>. Additionally,  
130 AVHRR-V6 *NDVI* products with a  $0.05^\circ \times 0.05^\circ$  spatial resolution and daily temporal resolution were  
131 also used ([https://www.ncei.noaa.gov/products/climate-data-records/normalized-difference-vegetation-](https://www.ncei.noaa.gov/products/climate-data-records/normalized-difference-vegetation-index)  
132 [index](https://www.ncei.noaa.gov/products/climate-data-records/normalized-difference-vegetation-index)). To minimize atmospheric and cloud pollution effects, the monthly maximum synthesis method  
133 (MVC) was adopted to calculate monthly-timescale *NDVI* datasets, which were then aggregated to the  
134 annual scale (Yao et al., 2018). Soil property data, including soil bulk density and soil texture, were  
135 extracted from the basic soil property dataset of the high-resolution China Soil Information Grids  
136 (<https://data.tpdc.ac.cn/zh-hans/data/e1ccd22c-348f-41a2-ab46-dd1a8ac0c955>). To explore the  
137 potential effect of soil organic matter on surface soil warming, soil organic carbon density (SOCD) data  
138 was used (Ding et al., 2016). The corresponding values for remote sensing data, reanalysis data, and  
139 upscaling results from literature, were extracted according to the latitude and longitude of the soil  
140 temperature observation sites and used to carry out the driving-factor attribution analysis.

141 Our study also involved consideration of the background atmospheric circulation of the TP. We  
142 selected nine atmospheric circulation indices comprising seven large-scale atmospheric and oceanic  
143 circulation patterns, namely the North Atlantic Oscillation (NAO), Arctic Oscillation (AO), Atlantic  
144 Multidecadal Oscillation (AMO), Pacific Decadal Oscillation (PDO) and El Niño Southern Oscillation  
145 (ENSO) (including the Nino3.4 sea surface temperature and multivariate ENSO index (MEI)). These  
146 were all accessed at <https://psl.noaa.gov/data/climateindices/list/>. Additionally, two summer monsoon  
147 indices were used: the South Asian summer monsoon index (SASMI) and the East Asian Summer  
148 Monsoon Index (EASMI) (Li and Zeng, 2002, 2003).

149 In addition, ground temperatures from depths of 3 m to 40 m at the permafrost borehole sites and



150 the mean annual ground temperature profile dataset at typical permafrost sites across the TP were  
151 obtained from the National Tibetan Plateau Data center (<https://data.tpdc.ac.cn/>) and the National  
152 Cryosphere Desert Data Center (<http://www.ncdc.ac.cn/portal/>).

### 153 2.2. Trend analysis

154 To examine temperature trends, we adopted the Mann-Kendall (M-K) nonparametric trend test  
155 (Mann, 1945; Kendall 1975). The Theil–Sen method was utilized to estimate the magnitude of the  
156 trend, while the nonparametric M–K method was employed to determine the significance of  
157 interannual trends in the temperature variables. The level of significance of trend alterations was  
158 expressed by a  $Z$  value, where  $Z < 0$  indicated a decrease and  $Z > 0$  an increase. In particular, these  
159 trends were considered statistically significant at the 99% confidence level ( $P < 0.01$ ) if  $|Z| \geq 2.58$  and  
160 at the 95% confidence level ( $P < 0.05$ ) if  $|Z| \geq 1.96$ . This nonparametric test is less sensitive to outliers  
161 and more accurate than the linear regression method, and thus is widely used to analyze  
162 hydrometeorological time-series data (Ding et al., 2018; Jiao et al., 2021). The regional averages of  
163 temperature indices were calculated as the arithmetic mean of the values at all the selected observation  
164 sites.

### 165 2.3. Statistical analysis

166 The Pearson correlation analysis method was used to identify the driving factors of TP ground  
167 warming. This method quantifies the degree of compactness by analyzing the magnitude of the linear  
168 relationship between two variables (Ding et al., 2019). A two-tailed version of Student's  $t$ -test was used  
169 to determine the statistical significance of the correlation coefficients at the significance levels  $P < 0.05$   
170 and  $P < 0.01$ . The annual maximum and minimum mean daily soil temperatures were calculated as



171 annual maximum temperature ( $T_{\max}$ , °C), and annual minimum temperature ( $T_{\min}$ , °C), respectively.  
172 Here, spring, summer, autumn and winter are defined as extending from March to May (MAM), June  
173 to August (JJA) September to November (SON) and December to the following February (DJF),  
174 respectively.

### 175 3. Results

#### 176 3.1. Regional annual tendencies and spatial patterns of soil temperature in multiple layers

177 Figure 2 and Table 1 depict the regional annual trends and statistical analyses of multi-layer soil  
178 temperatures in the Tibetan Plateau between 1981 and 2021. During this period, a statistically  
179 significant ( $P < 0.05$ ) warming trend was observed at depths ranging from 0 to 40 cm at the majority of  
180 sites (>80%) (Tab. 1). However, due to the limited time span of the observations at depths between 80  
181 and 160 cm, a higher percentage of sites exhibited non-significant warming trends at these depths. The  
182 linear tendencies of soil temperature at 0 cm depth ( $T_{s,0\text{cm}}$ ) in the TP region ranged from  $-0.24$  to  
183  $1.29$  °C/decade, with an average regional warming rate of  $0.51$  °C/decade ( $P < 0.01$ ) (Fig. 2a and Tab.  
184 1). The warming rates gradually decreased with increasing soil depth; the regional warming trends  
185 declined from  $0.47$  °C/decade at a depth of 5 cm to  $0.40$  °C/decade at 40 cm. The regional average  
186 warming rates of shallow soil between 0 and 20 cm were greater than that of air temperature (Fig. 2a).  
187 Additionally, the annual maximum soil temperature ( $T_{\max}$ ) warming rate generally increased with soil  
188 depth from the ground surface to a depth of 40 cm (Fig. 2d), whereas the warming rate of the minimum  
189 soil temperature ( $T_{\min}$ ) exhibited a decrease at greater depth (Fig. 2f). Notably, the  $T_{\max}$  warming rate  
190 exceeded that of  $T_{\min}$  between the depths of 5 and 40 cm, leading to an increase in the intra-annual  
191 variation of surface soil temperature across the whole region. The difference in annual mean



192 temperature between different soil depths was much smaller than the variation in annual maximum and  
193 minimum temperatures. These results indicate that the variation of the gradient of soil temperature with  
194 depth was greater during the coldest and warmest months.

195 Figure 3 and Figure S1 display the spatial distributions of the annual mean air temperature and  
196 layered soil temperature warming trends. Although there are some variations in the magnitudes of the  
197 trend changes in air temperature and soil temperature at depths of 0–40 cm, the spatial patterns of the  
198 warming trends remain largely consistent. Regionally, the relationships between trends in surface air  
199 temperature and soil temperature at depths between 0 and 40 cm are significant ( $P < 0.05$ ). However, the  
200 correlation efficiencies between air temperature and soil temperature warming rates gradually decrease  
201 with increasing soil depth, ranging from 0.72 at the ground surface to 0.42 at a depth of 40 cm (Fig. 4a).  
202 For  $T_{s_{0cm}}$ , the central and northeastern parts of the TP have experienced a higher increase in soil  
203 temperature than other areas. In contrast, the stations with relatively small warming rates are mainly  
204 located in the southern and southeastern regions of the TP, and almost all of the stations with  
205 insignificant positive trends are also situated in these areas (Fig. 3a). From the ground surface to 40 cm  
206 below ground, the number of effective observation sites decreased, and the temperature rising at the  
207 same site declined simultaneously. Due to the closely spaced measurement depths, the distribution  
208 patterns and magnitudes of the change trends of  $T_{s_{5cm}}$ ,  $T_{s_{10cm}}$  and  $T_{s_{20cm}}$  are very similar (Fig. S1 and  
209 Fig. 3b–c). However, the spatial distributions of the trends at 80–160cm differed substantially from the  
210 surface soil temperature because of the short observation time periods. Generally, in terms of individual  
211 station trends for depths between 80–160cm, upward trends were detected at approximately 60% of  
212 stations, while 20.9%–31.1% of stations passed the significance test at the 0.05 level (Table. 1). The  
213 few stations with lower significance negative tendencies were mainly in the southern TP. Pearson



214 correlation coefficients were calculated for the multi-year mean values and the related temperature  
215 trends during the observation period to clarify the spatial patterns between the air temperature and the  
216 layered soil temperature increase rates. The results show that the warming trends tend to be stronger at  
217 sites with lower multi-year mean temperatures, but the relationship was not significant ( $P>0.05$ ) for  
218 deeper soils (Fig. S2).

### 219 **3.2. Monthly and seasonal trend variability of layered soil temperature**

220 In the preceding sections, we examined the temporal and spatial variations of layered soil  
221 temperatures at an interannual scale, and found that the spatiotemporal change patterns exhibited both  
222 regularity and variability with soil depth. To elucidate the trend differences of monthly and seasonal  
223 variations in layered soil temperature, further exploration is required. To this end, we analyzed the  
224 regional average monthly trends for layered soil temperature for the period of 1981–2021. Our results  
225 demonstrate a significant warming trend in air temperature and layered soil temperature in all months  
226 on the TP (Fig. 5). Notably, the warming trend in soil temperature varies with month at different depths,  
227 but follows a regular pattern. Specifically, the monthly average warming trend of the ground surface  
228 (i.e.,  $T_{s\_0cm}$ ) was consistent with that of air temperature, with both reaching their maximum in  
229 February (Fig. 5a and b). However, the month with the maximum warming trend was gradually delayed  
230 to a later date, with increasing soil depth. More specifically, the months with the greatest average  
231 warming trend at 5 cm, 10 cm, 20 cm, and 40 cm soil depth were March, April, April, and June,  
232 respectively (Fig. 5c-f). These findings suggest that the warming of the surface soil is driven by the  
233 increasing temperature of the air near the surface, with the warming of the deeper soil lagging behind  
234 the surface soil.

235 In addition to analyzing the monthly results, we further examined the long-term variations in



236 seasonal soil temperatures. The results show a clear regularity between soil temperature in different  
237 layers and seasonal variation (Fig. 6). Specifically, during spring and summer, the temperature  
238 decreased with increasing soil depth, while during autumn and winter, the opposite trend was observed,  
239 with deeper soil layers exhibiting higher temperatures. These findings can be attributed to the storage  
240 and release of soil heat resulting from seasonal changes in land-atmosphere interactions. Furthermore,  
241 the temperature difference between the ground surface and the deepest soil layer was largest in summer  
242 and winter, and smallest in spring and autumn. With regards to seasonal trends, it appears that air  
243 temperature and soil temperature at shallow depths (between 0 and 40cm) significantly ( $P<0.05$ )  
244 increased in all seasons over the past four decades. The seasonal warming trend of the ground surface  
245 (i.e.,  $Ts_{0cm}$ ) remained consistent with the air temperature and was larger in the cold season, i.e.,  
246 autumn and winter, while the warming trend of the 5-40 cm soil layer was greater in the warm season,  
247 i.e., spring and summer. For the surface soil (between 5 and 40 cm) the warming trend gradually  
248 increased with increasing depth in spring and summer, whereas in autumn and winter, it showed a  
249 decreasing trend. However, the soil at depths between 80 and 160 cm showed a warming trend in  
250 almost all seasons, but the warming rates were small and insignificant ( $P>0.05$ ), probably due to the  
251 shorter period of observations for these depths.

### 252 **3.3. The impact of geographic location and altitude on layered soil temperatures**

253 The preceding analysis indicates a discernible spatial pattern in the warming rates of surface soils  
254 on the TP. For instance, stations with greater warming magnitudes at 0 cm are predominantly situated  
255 in the northeastern and central regions of the TP, as depicted in Figure 3a. Consequently, to  
256 comprehensively determine the potential impact of geographical location and topographic environment  
257 on the variation trends in air temperature and layered soil temperature, a correlation analysis was



258 conducted to examine the relationships between longitude, latitude, altitude, and temperature trends. As  
259 shown in Table 2, we observed a significant correlation between the trends of air temperature and  
260 layered soil temperatures with altitude in the TP region, indicating that the warming amplitude tends to  
261 be higher at higher altitudes. However, almost all the correlation coefficients between temperature  
262 increasing rates and longitude and latitude are not statistically significant at the 0.05 level, suggesting  
263 that longitude and latitude have minimal effects on the regional warming rates of surface soil in the TP  
264 area.

#### 265 **3.4. Impacts of environmental drivers and soil properties on surface soil warming**

266 The spatial variability of soil temperature increases is influenced by a range of environmental  
267 factors, including climate variables, snow depth and cover, vegetation, and soil properties. Owing to  
268 the highly consistent and similar soil temperature trends in the surface layer (0-40 cm) of the TP on  
269 both temporal and spatial scales, we chose to use the 20 cm soil depth (the middle of the surface soil  
270 layer) for our examination of the impact of environmental drivers and soil properties on surface soil  
271 warming. Our findings reveal a weak but non-significant ( $P>0.05$ ) positive correlation between soil  
272 warming and trend changes in precipitation and surface soil water content, indicating that the warming  
273 rate tends to be higher at sites with increased precipitation and soil water content (Fig. 7a and b). In  
274 contrast, the changing trends in snow depth and snow-cover days had negative associations with  
275 surface soil warming; that is, soil warming trends were greater at sites with decreasing snow depth or  
276 snow-cover days. However, the trend between changes in snow-cover days and soil warming was the  
277 only statistically significant one ( $P<0.05$ ). Vegetation changes can impact surface albedo and therefore  
278 surface heat gain. However, in this study, there was practically no discernible correlation between  
279 vegetation index trend changes and soil temperature increases, likely due to the locations of the



280 observation stations, which are primarily in eastern alpine meadow regions (Fig 7e). Further,  
281 downward long-wave radiation plays a crucial role in ground energy acquisition. Our analysis  
282 demonstrates a relatively weak, yet significant, positive correlation between downward long-wave  
283 radiation and soil temperature increase, suggesting that the rise in downward long-wave radiation could  
284 drive soil warming (Fig 7f). However, our results for soil properties showed that soil organic carbon  
285 content, soil bulk density, and soil texture had almost no association with soil temperature increases  
286 (Fig 7g-i).

### 287 **3.5. Association between atmospheric circulations and shallow soil warming**

288 Shallow soil warming reflects the overall regional ground energy balance and is closely related to  
289 regional atmospheric circulation patterns and changes in the climate system. To clarify the relationships  
290 between the variability of layered soil temperatures and large-scale climate systems, we analyzed the  
291 correlations between regional average annual change trends of layered soil temperatures and the AMO,  
292 AO, NAO, PDO, ENSO (MEI and Nino3.4), and summer monsoon indices (including SASMI and  
293 EASMI) (Table 3).

294 Table 3 shows that the shallow-soil warming trends have significant positive correlations with the  
295 AMO ( $P < 0.01$ ), weak significant negative correlations with PDO and MEI ( $P < 0.05$ ), and insignificant  
296 negative correlations with most of the remaining atmospheric circulation indices. These findings  
297 indicate that AMO has a strong impact on shallow soil warming on the TP at the annual scale.  
298 Additionally, we analyzed the long-term trends of  $T_{s,20cm}$  and AMO indices to further explore the  
299 possible mechanism by which the atmospheric circulation index influences surface soil warming. The  
300 results show that the annual variations of  $T_{s,20cm}$  have an almost perfect matching relationship with the  
301 phase change of AMO.



### 302 3.6. Ground temperature variations of the permafrost borehole site

303 The soil temperature observation sites analyzed above are primarily located in the seasonally  
304 frozen ground of the TP. The soil temperature results presented above only represent variations in near-  
305 surface ground temperature. However, the TP hosts the world's largest alpine permafrost zone outside  
306 of the polar regions, and therefore, we further integrated observation sites in the typical permafrost  
307 zone of the TP, analyzing changes in ground temperature from the surface to much deeper layers (i.e.,  
308 30-60m) to gain a more comprehensive understanding of ground temperature changes in the permafrost  
309 region of the TP.

310 Ground temperature at depths ranging from 3 m to 40 m showed greater warming trends at the  
311 lower temperature sites (Fig. 8). For instance, at a depth of 3 m, the warming rate was 1.2 °C/decade at  
312 the coldest site (QTB09), and 0.20 °C/decade at the warmest site (QTB11) (Fig. 8a). Moreover, the  
313 warming rate at the lowest and highest temperature sites at a depth of 30 m were 0.21 and  
314 0.10 °C/decade, respectively. The warming trends of ground temperatures at most sites gradually  
315 decreased with increasing depth, and the warming rate was minimal at the greatest measured depth of  
316 40 m (Fig. 8f). For example, at the WD4 site, the warming rate gradually decreased from  
317 0.27 °C/decade at a depth of 10 m to 0.06 °C/decade at a depth of 40 m. However, several sites  
318 exhibited anomalous warming trends with depth, which may be due to various local factors influencing  
319 soil temperature changes.

320 We conducted an additional analysis of the annual temporal variation of ground temperature  
321 profiles at several typical permafrost observation sites on the TP. Due to data sharing constraints, we  
322 only analyzed observations from between 2001 and 2010, but this short period should still basically  
323 reflect changes in permafrost ground temperature on the TP. We found that ground temperatures have



324 risen notably at all permafrost profiles since 2001 down to depths of 30m, 40m, or 60m in different  
325 sites (Fig. 9a-e). For most sites, record high ground temperatures were observed in 2010. The  
326 exceptions were QTB02 and QTB05 which might have been influenced by snow cover, resulting in a  
327 corresponding cooling change. The variation of ground temperature with depth and the trend of  
328 warming at different depths varied due to the influence of regional topography, climate, lithology, ice  
329 content, snow depth, and snow-cover duration. Based on the profiles of ground temperature variation,  
330 we found that 10 m was the approximate demarcation depth for QTB05, QTB06, and QTB15 (the  
331 depth above which the temperature sharply decreased and below which it gradually increased). For  
332 QTB01, the ground temperature increased continuously from the surface to the deep layer, while for  
333 QTB02, the temperature underwent a phase of warming, cooling, and re-warming. The surface ground  
334 temperature (at approximately 5 m depth) varied significantly with depth for all sites, whereas the  
335 deeper layers exhibited relatively weak variations. Furthermore, the warming trend decreased with  
336 increasing depth at all sites, and the low-temperature sites, such as QTB02 and QTB15, exhibited the  
337 most pronounced temperature increase at all depths (Fig. 9b and e). However, the site where the surface  
338 temperature was close to 0 °C, QTB06, was significantly different to the other sites, in that it was  
339 difficult to observe an obvious warming trend below 5 m depth (Fig. 9d).

#### 340 **4. Discussion**

##### 341 **4.1 A warmer climate has led to persistent and enhanced soil warming**

342 Our study shows a significant increase in soil temperatures in shallow ground on the TP from  
343 1981 to 2021, with most sites exhibiting statistically significant ( $P < 0.05$ ) warming trends. The trend of  
344 soil warming gradually decreases with depth, with regional increasing trends ranging from



345 0.47 °C/decade at a depth of 5 cm to 0.40 °C/decade at 40 cm. We also found that warming trends tend  
346 to be stronger at sites with lower mean temperatures or higher elevations. Overall, our study provides a  
347 comprehensive evaluation of the evolution of soil temperature on the TP by quantifying spatial and  
348 temporal trends in multi-layer shallow ground temperatures.

349 The continuous warming of shallow soils on the TP over the past few decades is noteworthy, and,  
350 taken together with similar warming trends observed in various regions across the globe (Chen et al.,  
351 2021c; Dorau et al., 2022; Gao et al., 2022; Qian et al., 2011; Wang et al., 2018), is a clear indication of  
352 global warming. The spatial warming trend of the ground surface is strongly correlated with air  
353 temperature and gradually decreases with depth (Fig. 4a). This indicates that soil warming is driven by  
354 air temperature, with heat transfer and decay progressing downwards into the soil following surface  
355 warming (Chen et al., 2021a; Wang et al., 2021). As a result, the temperature of the deep soil lags  
356 behind the surface warming, and the magnitude of warming becomes progressively smaller with depth  
357 due to the filtering effect of the soil layers above (Smith et al., 2022). Monthly and seasonal trend  
358 variability of multi-layered soil temperature provide a better indication of the transmission and decline  
359 of soil warming trends from the surface to the deeper layers. For example, the fluctuations in the  
360 monthly average warming trend of the ground surface were almost wholly consistent with those of air  
361 temperature (Fig. 5). However, the month in which the maximum warming trend occurred was  
362 regularly delayed to a later date at deeper soil depths. Seasonal variation in soil temperature in different  
363 layers is due to the superposition and transfer effect of monthly trends. As a result of this lag-effect of  
364 heat transfer, although the maximum warming trends of the ground surface occurred in winter, the  
365 seasonal warming rate of the soil at a depth of 40 cm reached its maximum in summer.

366 Although air temperature is the main controlling factor of soil warming, the heat transfer process



367 from atmospheric conditions to shallow ground will be affected by the insulating effects of vegetation,  
368 snow cover and other factors (Smith et al., 2022). The deepest soil layers respond less to atmospheric  
369 warming due to environmental factors like soil texture, soil organic matter, and soil water content. This  
370 leads to a gradual weakening of the correlation between surface air and soil warming rates with  
371 increasing depth (Fig. 4a). However, in this study, only snow-cover days and downward long-wave  
372 radiation were significantly correlated with surface soil temperature trends (Fig. 7). Snow-cover limits  
373 heat loss from the ground surface, affecting the response of shallow ground thermal conditions to  
374 surface air warming (Chen et al., 2021b). However, the snow cover on the TP has had a significant  
375 downward trend in recent decades under the background of intense climate warming, with reduced  
376 depth and shortened duration (Xu et al., 2017). The snow cover on the TP is mainly concentrated in  
377 winter and spring. The delay in the start of the snow-covered period and the associated decrease in the  
378 number of snow-cover days in winter weakens the ground thermal insulation effect, slowing down the  
379 trend of increasing temperature of the shallow soil. In contrast, the advance of the end of the snow-  
380 cover period in spring allows the ground to receive more solar radiation and absorb more heat,  
381 intensifying the warming trend of the shallow soil layers (Qian et al., 2011). This asynchronous  
382 response of soil temperature to snow-cover changes in different seasons leads to a weak negative  
383 correlation between the number of days with snow cover and the rate of surface soil temperature  
384 increase on an interannual scale (Fig. 7d).

385 Atmospheric downward longwave radiation (DLR) is an essential part of the surface energy  
386 balance and a basic indicator of the effect of atmospheric greenhouse gases on climate warming (Tang  
387 et al., 2021). The increase in DLR, seen here, allows the ground surface layer to absorb more heat,  
388 driving a sustained warming of the shallow soil layer. In recent decades, the *NDVI* of the TP has shown



389 a continuous increasing trend under the warming and wetting climate (Shen et al., 2022). This  
390 improvement of the vegetation increases solar radiation absorption by reducing albedo, accelerating  
391 surface warming. However, at the same time, evaporative cooling induced by vegetation growth  
392 weakens surface warming, and so, overall, vegetation growth generally has little influence on shallow  
393 soil warming (Shen et al., 2015). As the largest region of permafrost in the mid-latitudes, the TP has a  
394 huge store of soil organic carbon (Taihua et al., 2020). Soil organic matter has a low thermal diffusivity,  
395 leading to a weakening of the warming rate of shallow soil (Zhu et al., 2019). However, we found no  
396 obvious relationship between the warming rate of shallow soil and soil organic carbon content. This  
397 may be due to the limited accuracy of the soil organic carbon data extracted from other up-scale studies  
398 and the fact that the ground temperature observation stations were mainly located in the central and  
399 eastern regions of the plateau.

400 In addition to the environmental driving factors discussed above, the heterogeneity of topography  
401 and atmospheric circulations may also impact the changing trends in soil temperatures. Our results  
402 show a positive correlation between shallow soil warming and altitude, indicating that warming trends  
403 tend to be greater at higher altitudes (Table 2). The increase in soil warming rates with elevation is  
404 primarily due to elevation-dependent surface air warming, which may be related to snow/ice-albedo  
405 feedback, aerosol feedback, and cloud feedback (You et al., 2020). Furthermore, the number of snow-  
406 covered days tends to decrease significantly with increasing altitude (Fig. S3), resulting in a lower  
407 ground albedo and increased solar radiation absorption at the surface, exacerbating soil warming in  
408 regions of high elevation (Zhang et al., 2022). However, in this study, the observation sites were of  
409 limited number with an uneven distribution: a full analysis of the mechanisms of soil temperature



410 increasing with altitude would require an increase in in-situ measurements and corresponding  
411 theoretical support.

412 Large-scale atmospheric circulations may modulate the rate of shallow ground warming on the TP  
413 through their effects on near-surface air temperature and the ground-surface radiation balance. Our  
414 results demonstrate strong positive correlations between long-term trends of  $T_{s,20cm}$  and the AMO  
415 indices (Table 3). The AMO index describes quasi-periodic warm and cold anomalies of sea surface  
416 temperatures in the North Atlantic, which can cause prominent climate changes globally through  
417 atmosphere–ocean–sea ice interactions (Hao et al., 2015; Schlesinger and Ramankutty, 1994). Previous  
418 research has shown that sea surface temperature anomalies in the North Atlantic can cause anticyclonic  
419 circulation anomalies and have a crucial impact on the variability in surface air temperature in many  
420 places around the world through teleconnection (Ding et al., 2020; Li et al., 2020; Zhang et al., 2020a).  
421 Furthermore, weak, significant negative correlations between shallow soil warming rates and the  
422 Pacific Decadal Oscillation (PDO), North Atlantic Oscillation (NAO), and Multivariate ENSO Index  
423 (MEI) suggest that large-scale atmospheric circulations in other regions may also influence shallow  
424 ground warming over the TP through teleconnection. The physical mechanisms of atmospheric  
425 circulations regulating ground warming are complex; they may affect surface warming rates by  
426 influencing regional changes in solar radiation, aerosols, air pressure, precipitation, and particularly air  
427 temperature, thereby causing changes in the ground surface energy balance.

#### 428 **4.2 Potential mechanisms of permafrost-profile warming dynamics**

429 Consistent with shallow soil warming in the seasonal permafrost zone, permafrost temperatures  
430 and dynamics at typical sites have increased steadily over the past two decades (Fig. 8 and 9), in  
431 alignment with observed warming in permafrost regions globally (Biskaborn et al., 2019; Eitzelmüller



432 et al., 2020). However, the magnitudes of warming at different permafrost sites vary due to the  
433 regulating effects of regional environmental attributes, such as snow cover, ice, content, vegetation and  
434 organic-layer thickness. Maximum temperature increases at various depths from 3 m to 40 m typically  
435 occur at the colder sites (Fig. 8), mainly due to a faster warming rate of surface air temperature at  
436 colder sites. In addition, due to the filtering and "memory" functions of the ground, the interannual  
437 temperature fluctuations are greater at shallower ground levels and decrease progressively with depth  
438 (Smith et al., 2022). Similarly, the warming trend gradually decreases with depth, becoming quite weak  
439 at depths such as 40 m for example (Fig. 8f). The ground thermal regime and its variability across the  
440 typical permafrost sites on the TP can be explained more clearly by considering the temperature  
441 variation of the ground profiles. Our findings reveal that the warming trend gradually decreases with  
442 depth and is most prominent at sites with lower surface temperatures, such as QTB02 and QTB15,  
443 followed by sites with higher surface temperatures, such as QTB05. However, sites with surface  
444 temperatures close to 0 °C, such as QTB06, showed a negligible increase in temperature down the  
445 profile (Fig. 9). The primary mechanism behind this phenomenon is the latent heat effect that occurs  
446 during permafrost thawing. This effect consumes a significant amount of the energy used for warming,  
447 making it difficult to detect changes in the ground temperature signal across the profile at sites with  
448 surface temperatures close to 0 °C (Etzelmüller et al., 2020).

449 Our observations show significant variations in ground temperature changes with depth across the  
450 different sites (Fig. 9). This variability can be attributed to differences in permafrost properties such as  
451 ice and organic matter content, and rock composition, which lead to variations in thermal conductivity  
452 and thus the regulation of vertical heat transfer within the permafrost (Etzelmüller et al., 2020; Zhu et  
453 al., 2019). The combined effects of surface buffer zones and differences in subsurface thermal



454 conductivity determine the vertical variation in ground temperature in different permafrost regions.  
455 However, since current permafrost ground temperature monitoring is sporadically distributed across the  
456 TP, the conclusions derived from this analysis may not fully explain the potential mechanisms of  
457 permafrost ground warming dynamics.

#### 458 **4.3 Implications of persistent increases in ground temperature**

459 According to our study, multi-layered soil temperature and ground temperatures in typical  
460 permafrost zones on the Tibetan Plateau (TP) have experienced continuous warming in recent decades,  
461 with the warming being more pronounced in low temperature and high elevation areas. This sustained  
462 increase in ground temperature has resulted in significant environmental changes that have profound  
463 impacts on multi-sphere coupling and changes in the TP (Yang et al., 2019; Yao et al., 2022; Yao et al.,  
464 2019). Notably, low temperature and high altitude areas are also the most concentrated regions of  
465 permafrost and glacier distribution on the TP. Persistent ground warming in these areas will aggravate  
466 permafrost degradation by accelerating the melting of ice, thickening the active layer and expanding  
467 the distribution of thermokarst landforms, etc. (Mu et al., 2020). For instance, the lower altitudinal  
468 limit of permafrost distribution has been continuously rising, and the total area of permafrost on the TP  
469 has shrunk by about 30% in the last 50 years due to persistent ground warming (Cheng et al., 2012;  
470 Zou et al., 2017). In the permafrost region of the TP, the cold environment sequesters a large amount of  
471 soil organic carbon (Ding et al., 2016). The degradation of permafrost caused by rising ground  
472 temperature accelerates the exposure, decomposition and lateral transport of this organic carbon to  
473 rivers, which leads to the acceleration of greenhouse gas emissions possibly enhancing climate  
474 warming in a positive feedback effect (Liu et al., 2022; Zhang et al., 2020b). Further, the sustained  
475 increase in ground temperature in the glacier areas of the TP will accelerate glacier melting and



476 collapse, which will promote lake expansion and increase runoff in the basin in the short term. In the  
477 long term, however, ice avalanche debris flow and severe geological disasters will also increase,  
478 leading to an imbalance of the Asian water tower (Zheng et al., 2021). The continuous rise of ground  
479 temperature will accelerate water evaporation and the decline of groundwater levels in this globally  
480 important area of alpine wetland, resulting in a gradual drying and degradation of the wetlands, and the  
481 loss of ecohydrological functions (Shen et al., 2019).

482 In summary, persistent ground warming accelerates the instability of the TP cryosphere.  
483 Understanding the ground temperature changes on the TP is critical to accurately assess the regional  
484 carbon and water cycles and their feedbacks to climate change. Currently, however, ground temperature  
485 observations are inadequate, model simulation mechanisms are insufficient, and result evaluations have  
486 large uncertainties. Specifically, the monitoring of soil temperature on the TP mainly relies on  
487 meteorological stations in the central and eastern parts of the plateau, while observation of deep  
488 permafrost ground temperature is only sporadically distributed in the permafrost area (Fig. 1). Due to  
489 the harsh environmental conditions and limitations on accessibility, *in-situ* observations of ground  
490 temperature in the western permafrost region are extraordinarily scarce. Additionally, the complex  
491 subsurface structure introduces numerous factors affecting internal heat transfer, and models often  
492 cannot account for the heterogeneity of these factors when simulating regional ground heat transfer.  
493 Therefore, there are often large errors in simulations of regional soil warming. To remove these  
494 limitations on the progress of research in this area, it is necessary to intensify monitoring networks of  
495 ground temperature in the central and western plateau regions. Observational results should be  
496 continuously used to evaluate and optimize model outputs to improve their accuracy, and satellite  
497 remote sensing technology should be strengthened to improve the accuracy of regional estimates.



## 498 5. Conclusions

499 We investigated multi-layered soil warming trends, permafrost ground temperature profiles, and  
500 their driving factors on the Tibetan Plateau. Our study demonstrates that shallow soil layers on the TP  
501 warmed significantly from 1981 to 2021, with trends decreasing with depth. Areas with lower annual  
502 mean temperatures and higher elevations had more pronounced warming trends. The change in the  
503 monthly average warming trend of the ground surface was consistent with changes in air temperature,  
504 but with increasing soil depth, the month in which the maximum warming trend occurred was delayed  
505 to a later date. The seasonal warming trends of the ground surface and air temperature were larger in  
506 the cold season, i.e., autumn and winter, while the warming trend of the soil in the 5–40 cm layer was  
507 greater in the warm season, i.e., spring and summer. Out of the multiple factors, in addition to air  
508 temperature, that may affect sustained soil warming, we only found significant positive correlations  
509 with soil warming rates for snow-cover days and downward longwave radiation. The Atlantic Multi-  
510 decadal Oscillation (AMO) strongly influenced shallow soil warming at annual scales. Our analysis  
511 also suggests persistent warming in typical permafrost profiles although there is spatial heterogeneity in  
512 these results. Consistent with the warming pattern of the surface soil, the permafrost profile warming  
513 rate was intense in the surface layer and decreased with increasing depth, becoming quite minimal at  
514 the deepest observed depth of 40 m. The extent and variation of profile warming with depth are  
515 influenced by multiple factors, including local climate, lithology, and elevation. Given the numerous  
516 adverse effects of continued ground temperature rise on the TP cryosphere, we strongly urge intensified  
517 field monitoring of ground temperature in the permafrost region, combined with satellite remote  
518 sensing technology, and the development of accurate subsurface heat transport models, suitable for the  
519 plateau, to improve our understanding of the implications of rapidly warming ground.



520 **Competing interests**

521 The contact author has declared that none of the authors has any competing interests.

522 **Acknowledgements**

523 The authors express their gratitude to all individuals who contributed to the ground temperature  
524 observations in this study. We are grateful to Beiluhe Observation and Research Station on Frozen Soil  
525 Engineering and Environment in Qinghai-Tibet Plateau for providing the experimental sites and  
526 relevant supports. This study is supported by the Second Tibetan Plateau Scientific Expedition and  
527 Research Program (2022QZKK0101), the National Natural Science Foundation of China (42022004),  
528 the Chinese Academy of Sciences (CAS) Project for Young Scientists in Basic Research (YSBR-037),  
529 Science and Technology Major Project of Tibetan Autonomous Region of China  
530 (XZ202201ZD0005G04) and the West Light Scholar of Chinese Academy of Sciences (xbzg-zdsys-  
531 202202). Code/Data availability: The data are available from the corresponding author on reasonable  
532 request. Author contributions: Conceptualization: J.D., Y.W., S.P. Methodology: Y.W. Investigation:  
533 Y.W. Visualization: Y.W. and J.D. Supervision: J.D., and S.P. Writing—original draft: Y.W. Writing—  
534 review and editing: Y.W., J.D., and S.P.

535 **References**

- 536 Biskaborn, B.K. *et al.*, Permafrost is warming at a global scale, *Nat Commun* **10**(2019), p. 264.
- 537 Cao, B. *et al.*, Thermal Characteristics and Recent Changes of Permafrost in the Upper Reaches of the  
538 Heihe River Basin, Western China, *Journal of Geophysical Research: Atmospheres*(2018).
- 539 Chen, L., Aalto, J., Luoto, M., Decadal Changes in Soil and Atmosphere Temperature Differences  
540 Linked With Environment Shifts Over Northern Eurasia, *Journal of Geophysical Research:*  
541 *Earth Surface* **126**(2021a).



- 542 Chen, L., Aalto, J., Luoto, M., Observed Decrease in Soil and Atmosphere Temperature Coupling in  
543 Recent Decades Over Northern Eurasia, *Geophysical Research Letters* **48**(2021b).
- 544 Chen, L., Aalto, J., Luoto, M., Significant shallow–depth soil warming over Russia during the past  
545 40 years, *Global and Planetary Change* **197**(2021c).
- 546 Cheng, W., Zhao, S., Zhou, C., Chen, X., Simulation of the Decadal Permafrost Distribution on the  
547 Qinghai-Tibet Plateau (China) over the Past 50 Years, *Permafrost and Periglacial Processes*  
548 **23**(2012), pp. 292-300.
- 549 Ding, J. *et al.*, The permafrost carbon inventory on the Tibetan Plateau: a new evaluation using deep  
550 sediment cores, *Glob Chang Biol* **22**(2016), pp. 2688-2701.
- 551 Ding, Z., Lu, R., Wang, Y., Spatiotemporal variations in extreme precipitation and their potential  
552 driving factors in non-monsoon regions of China during 1961–2017, *Environmental Research*  
553 *Letters* **14**(2019).
- 554 Ding, Z. *et al.*, Asymmetric trends of extreme temperature over the Loess Plateau during 1998–2018,  
555 *International Journal of Climatology* **41**(2020).
- 556 Ding, Z., Wang, Y., Lu, R., An analysis of changes in temperature extremes in the Three River  
557 Headwaters region of the Tibetan Plateau during 1961–2016, *Atmospheric Research*  
558 **209**(2018), pp. 103-114.
- 559 Dorau, K., Bamminger, C., Koch, D., Mansfeldt, T., Evidences of soil warming from long-term trends  
560 (1951–2018) in North Rhine-Westphalia, Germany, *Climatic Change* **170**(2022).
- 561 Eitzelmüller, B. *et al.*, Twenty years of European mountain permafrost dynamics—the PACE legacy,  
562 *Environmental Research Letters* **15**(2020).
- 563 Li, Y. *et al.*, Analysis on the temporal and spatial characteristics of the shallow soil temperature of the



- 564 Qinghai-Tibet Plateau, *Scientific Reports* **12**(2022).
- 565 Hao, X., He, S., Wang, H., Asymmetry in the response of central Eurasian winter temperature to AMO,  
566 *Climate Dynamics* **47**(2015), pp. 2139-2154.
- 567 Hjort, J. *et al.*, Impacts of permafrost degradation on infrastructure, *Nature Reviews Earth &*  
568 *Environment* **3**(2022), pp. 24-38.
- 569 Intergovernmental Panel on Climate Change Climate change 2021: the physical science basis V.  
570 Masson-Delmotte, P. Zhai, A. Pirani (Eds.), Contribution of Working Group I to the sixth  
571 assessment report of the Intergovernmental Panel on Climate Change, Cambridge University  
572 Press, Cambridge (2021)
- 573 Jiao, W. *et al.*, Observed increasing water constraint on vegetation growth over the last three decades,  
574 *Nature Communications* **12**(2021).
- 575 Li, J., Zeng, Q., A unified monsoon index, *Geophysical Research Letters* **29**(2002), pp. 115-111-115-  
576 114.
- 577 Li, J., Zeng, Q., Anewmonsoon index and the geographical distribution of the global monsoons,  
578 *Advances in Atmospheric Sciences* **20**(2003), pp. 299-302.
- 579 Li, Z. *et al.*, A robust relationship between multidecadal global warming rate variations and the Atlantic  
580 Multidecadal Variability, *Climate Dynamics* **55**(2020), pp. 1945-1959.
- 581 Liu, F. *et al.*, Divergent changes in particulate and mineral-associated organic carbon upon permafrost  
582 thaw, *Nature Communications* **13**(2022).
- 583 Melo-Aguilar, C. *et al.*, Near-surface soil thermal regime and land–air temperature coupling: A case  
584 study over Spain, *International Journal of Climatology* **42**(2022), pp. 7516-7534.
- 585 Mu, C. *et al.*, The status and stability of permafrost carbon on the Tibetan Plateau, *Earth-Science*



- 586 *Reviews* **211**(2020).
- 587 Petersen, G.N., Trends in soil temperature in the Icelandic highlands from 1977 to 2019, *International*  
588 *Journal of Climatology* **42**(2021), pp. 2299-2310.
- 589 Qian, B., Gregorich, E.G., Gameda, S., Hopkins, D.W., Wang, X.L., Observed soil temperature trends  
590 associated with climate change in Canada, *Journal of Geophysical Research* **116**(2011).
- 591 Schlesinger, M.E., Ramankutty, N., An oscillation in the global climate system of period 65–70 years,  
592 *Nature* **367**(1994), pp. 723–726.
- 593 Shen, G., Yang, X., Jin, Y., Xu, B., Zhou, Q., Remote sensing and evaluation of the wetland ecological  
594 degradation process of the Zoige Plateau Wetland in China, *Ecological Indicators* **104**(2019),  
595 pp. 48-58.
- 596 Shen, M. *et al.*, Evaporative cooling over the Tibetan Plateau induced by vegetation growth,  
597 *Proceedings of the National Academy of Sciences* **112**(2015), pp. 9299-9304.
- 598 Shen, M. *et al.*, Plant phenology changes and drivers on the Qinghai–Tibetan Plateau, *Nature Reviews*  
599 *Earth & Environment* **3**(2022), pp. 633-651.
- 600 Shi, X. *et al.*, Long-term changes in layered soil temperature based on ground measurements in Jiangsu  
601 Province, China, *International Journal of Climatology* **41**(2021), pp. 2996-3009.
- 602 Smith, S.L., O’Neill, H.B., Isaksen, K., Noetzli, J., Romanovsky, V.E., The changing thermal state of  
603 permafrost, *Nature Reviews Earth & Environment* **3**(2022), pp. 10-23.
- 604 Taihua, W. *et al.*, Permafrost thawing puts the frozen carbon at risk over the Tibetan Plateau, *Science*  
605 *Advances* **6**(2020), p. eaaz3513.
- 606 Tang, W., Qin, J., Yang, K., Zhu, F., Zhou, X., Does ERA5 outperform satellite products in estimating  
607 atmospheric downward longwave radiation at the surface?, *Atmospheric Research* **252**(2021).



- 608 Wang, L. *et al.*, Maximum and Minimum Soil Surface Temperature Trends Over China, 1965-2014,  
609 *Journal of Geophysical Research: Atmospheres* **123**(2018), pp. 2004-2016.
- 610 Wang, X. *et al.*, Contrasting characteristics, changes, and linkages of permafrost between the Arctic and  
611 the Third Pole, *Earth-Science Reviews* **230**(2022).
- 612 Wang, X. *et al.*, Response of shallow soil temperature to climate change on the Qinghai-Tibetan  
613 Plateau, *International Journal Of Climatology* **41**(2021).
- 614 Wang, Z. *et al.*, Temperature effect on erosion-induced disturbances to soil organic carbon cycling,  
615 *Nature Climate Change* **13**(2023), pp. 174-181.
- 616 Xu, W., Ma, L., Ma, M., Zhang, H., Yuan, W., Spatial–Temporal Variability of Snow Cover and Depth  
617 in the Qinghai–Tibetan Plateau, *Journal of Climate* **30**(2017), pp. 1521-1533.
- 618 Yang, M., Wang, X., Pang, G., Wan, G., Liu, Z., The Tibetan Plateau cryosphere: Observations and  
619 model simulations for current status and recent changes, *Earth-Science Reviews* **190**(2019), pp.  
620 353-369.
- 621 Yao, T., Thompson, L., Chen, D., Piao, S., Reflections and future strategies for Third Pole Environment,  
622 *Nature Reviews Earth & Environment* **3**(2022), pp. 608-610.
- 623 Yao, T. *et al.*, Recent Third Pole’s Rapid Warming Accompanies Cryospheric Melt and Water Cycle  
624 Intensification and Interactions between Monsoon and Environment: Multidisciplinary  
625 Approach with Observations, Modeling, and Analysis, *Bulletin of the American*  
626 *Meteorological Society* **100**(2019), pp. 423-444.
- 627 Yao, Y. *et al.*, A new estimation of China’s net ecosystem productivity based on eddy covariance  
628 measurements and a model tree ensemble approach, *Agricultural and Forest Meteorology*  
629 **253-254**(2018), pp. 84-93.



- 630 You, Q. *et al.*, Elevation dependent warming over the Tibetan Plateau: Patterns, mechanisms and  
631 perspectives, *Earth-Science Reviews* **210**(2020).
- 632 Zhang, G., Zeng, G., Li, C., Yang, X., Impact of PDO and AMO on interdecadal variability in extreme  
633 high temperatures in North China over the most recent 40-year period, *Climate Dynamics*  
634 **54**(2020a), pp. 3003-3020.
- 635 Zhang, H. *et al.*, Snow cover persistence reverses the altitudinal patterns of warming above and below  
636 5000 m on the Tibetan Plateau, *Science of The Total Environment* **803**(2022).
- 637 Zhang, H., Yuan, N., Ma, Z., Huang, Y., Understanding the Soil Temperature Variability at Different  
638 Depths: Effects of Surface Air Temperature, Snow Cover, and the Soil Memory, *Advances in*  
639 *Atmospheric Sciences* **38**(2021), pp. 493-503.
- 640 Zhang, L. *et al.*, Significant methane ebullition from alpine permafrost rivers on the East Qinghai–Tibet  
641 Plateau, *Nature Geoscience* **13**(2020b), pp. 349-354.
- 642 Zhao, L., Wu, Q., Marchenko, S.S., Sharkhuu, N., Thermal state of permafrost and active layer in  
643 Central Asia during the international polar year, *Permafrost and Periglacial Processes*  
644 **21**(2010), pp. 198-207.
- 645 Zhang, L. *et al.*, Changing climate and the permafrost environment on the Qinghai-Tibet (Xizang)  
646 plateau, *Permafrost and Periglacial Processes* **31**(2020), pp. 396-405.
- 647 Zheng, G. *et al.*, Increasing risk of glacial lake outburst floods from future Third Pole deglaciation,  
648 *Nature Climate Change* **11**(2021), pp. 411-417.
- 649 Zhu, D. *et al.*, Controls of soil organic matter on soil thermal dynamics in the northern high latitudes,  
650 *Nature Communications* **10**(2019).
- 651 Zou, D. *et al.*, A new map of permafrost distribution on the Tibetan Plateau, *The Cryosphere* **11**(2017),



652 pp. 2527-2542.

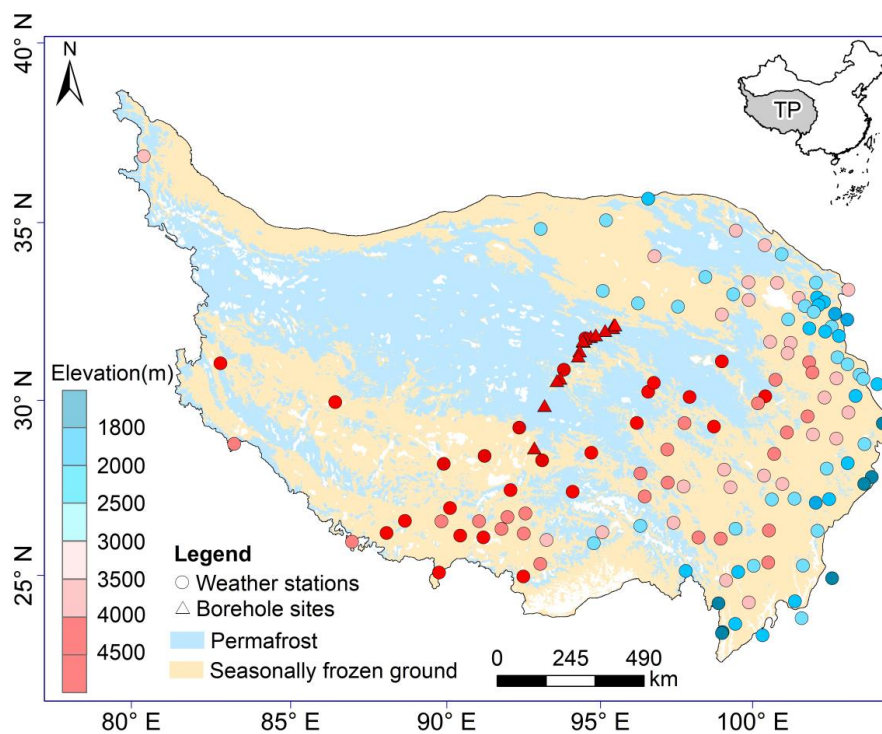
653

654

655

656

657 **Figures**



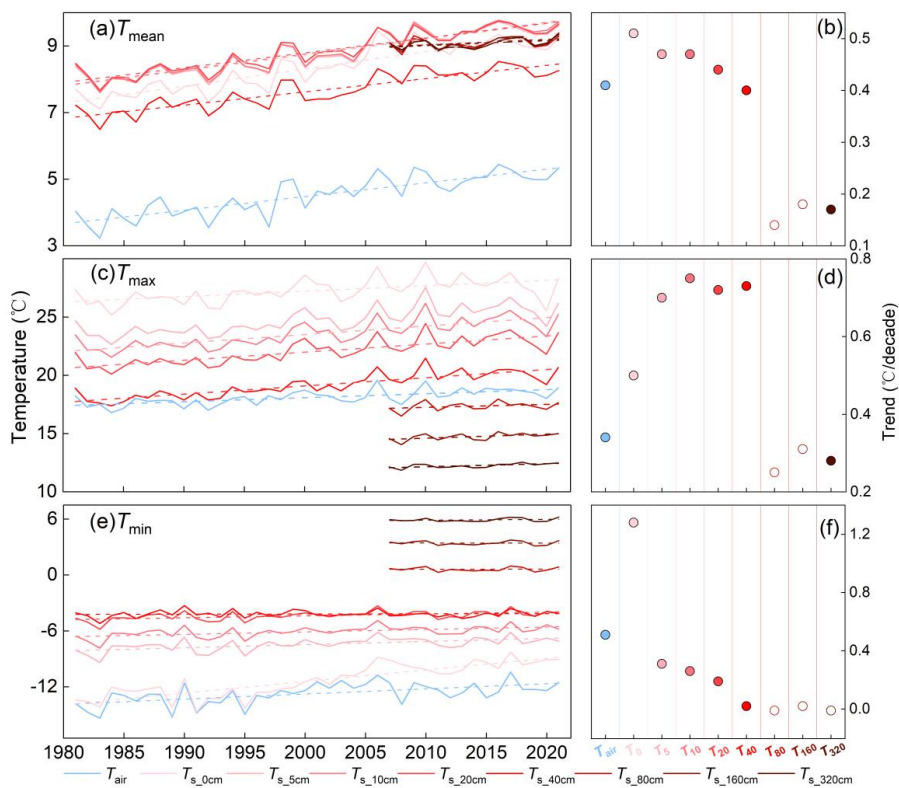
658

659 **Fig. 1.** Distribution of ground temperature observation sites in the permafrost regions of the Tibetan

660 Plateau.

661

662



663

664 **Fig. 2.** Regional average, maximum, and minimum annual air temperature ( $T_{\text{mean}}$ ,  $T_{\text{max}}$ ,  $T_{\text{min}}$ ) and

665 layered soil temperature series from 1981 to 2021.

666

667

668

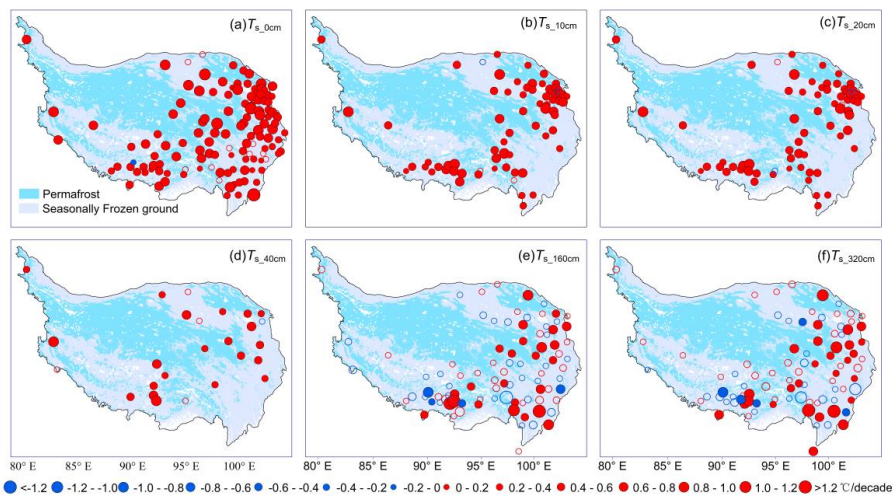
669

670

671

672

673



674

675 **Fig. 3.** Spatial patterns of trends in layered soil temperatures from 1981 to 2021. The hollow blue

676 circles and red circles in the figure represent the decrease and increase trend, respectively.

677

678

679

680

681

682

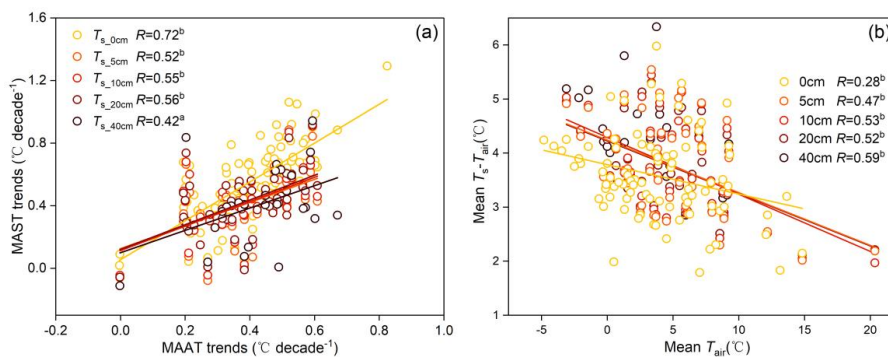
683

684

685

686

687



688

689 **Fig. 4.** Linear relationships between (a) trends in mean annual air temperature (MAAT) and mean  
690 annual soil temperatures (MASTs), and (b) the regional average MAAT and annual difference between  
691 MAST and MAAT, at depths of 0-40 cm.

692

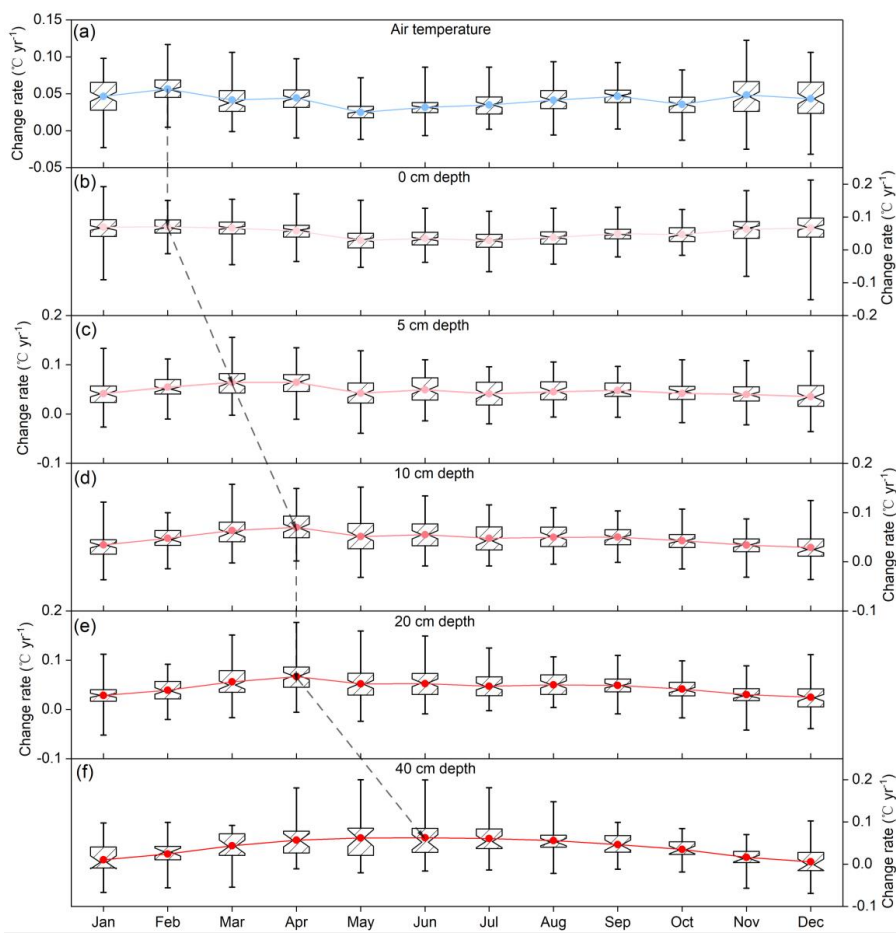
693

694

695

696

697

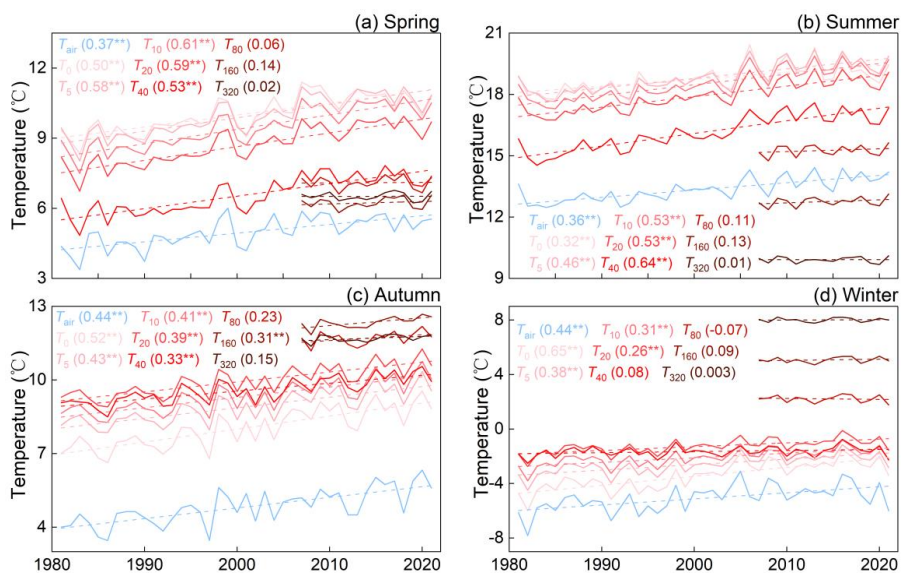


698

699 **Fig. 5.** Regional average monthly trends for air temperature and layered soil temperatures for 1981–

700 2021. The dashed line with arrows connects the months with the highest temperature trend each year.

701



702

703 **Fig. 6.** Regional average of seasonal series for air temperature and layered soil temperatures over the  
 704 period 1981–2021.

705

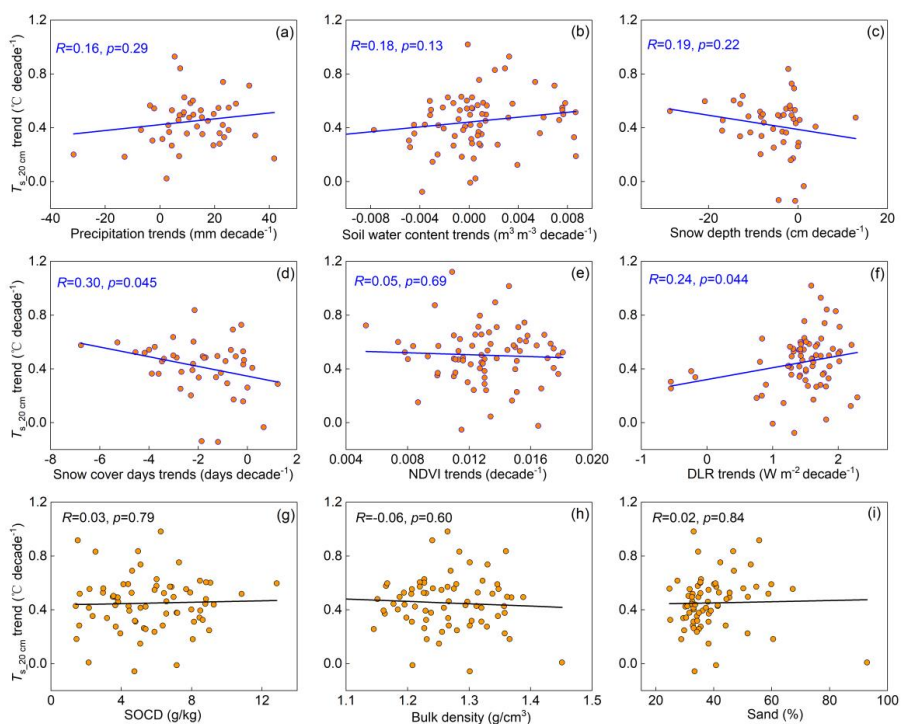
706

707

708

709

710



711

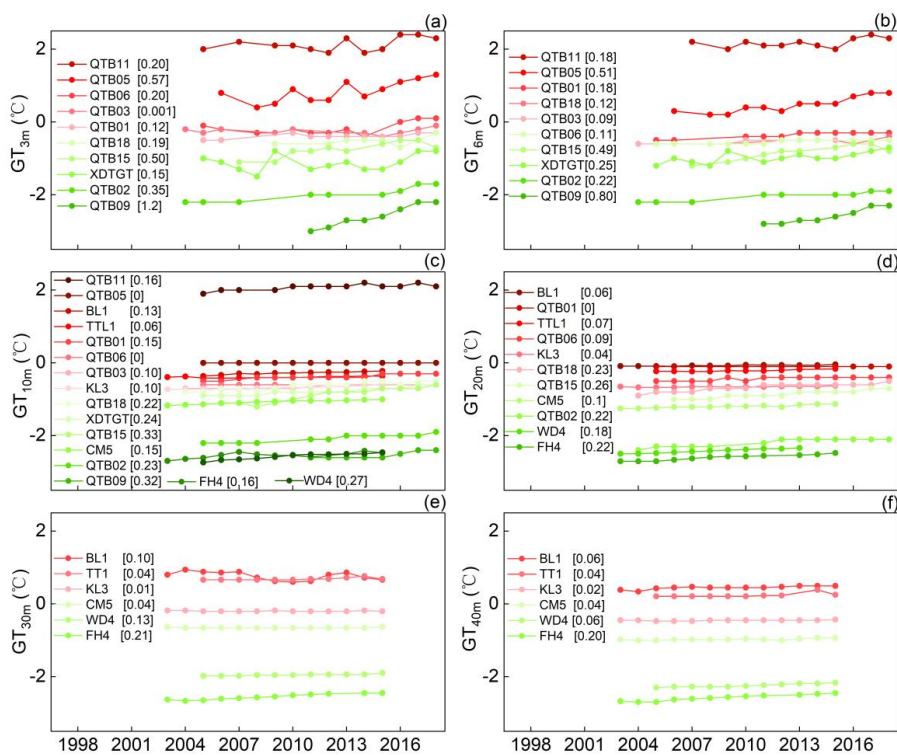
712 **Fig. 7.** Impacts of environmental drivers and soil properties on surface soil warming at a depth of 20

713 cm. The abbreviations *NDVI*, *DLR*, and *SOCD* refer to Normalized Difference Vegetation Index,

714 Downward Longwave Radiation, and Soil Organic Carbon Density, respectively.

715

716



717

718 **Fig. 8.** Changes in annual ground temperature (GT) from shallow ground (3m) to the deep layer (40m)

719 at compiled permafrost borehole sites. The values in brackets represent the increase/decrease trend

720 during the observed period.

721

722

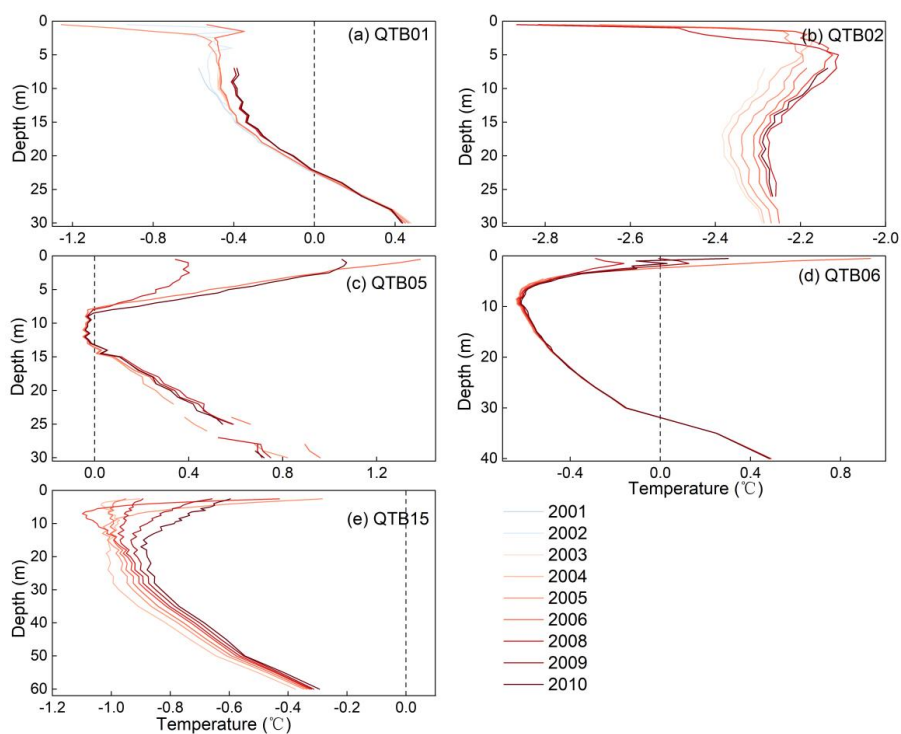
723

724

725

726

727



728

729 **Fig. 9.** Mean annual ground temperature profiles at typical permafrost sites on the Tibetan Plateau from

730 2000 to 2010. The dash lines are the longitudinal 0 °C line.

731

732

733

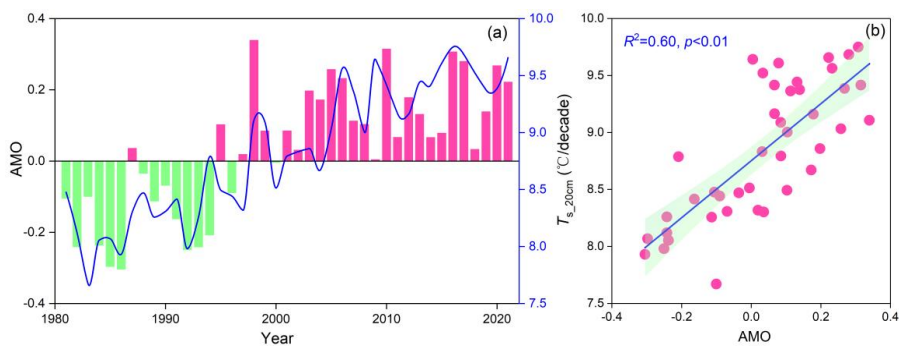
734

735

736

737

738



739

740 **Fig. 10.** Long-term trends of the Atlantic Multi-decadal Oscillation (AMO) indices and the 20 cm deep

741 soil temperature ( $T_{s,20\text{cm}}$ ) over the period 1981–2021.

742

743

744

745

746

747

748

749

750

751

752

753

754

755



756 **Tables**

757 **Table 1.** Regional decade-scale changes and the number of stations showing statistically significant (S)  
 758 trends (significant at the 0.05 level) in air temperature and layered soil temperatures.

Indices	Unit	Range of regional trends (mean) (decade <sup>-1</sup> )	Percentage of stations with S trends (%)	
			Increasing trend (S)	Decreasing trend (S)
$T_{\text{air}}$	°C	-0.003 ~ 0.82 (0.41)	97.8 (97.8)	2.2 (2.2)
$T_{s\_0\text{cm}}$	°C	-0.24 ~ 1.29 (0.51)	98.4 (89.8)	1.6 (0.8)
$T_{s\_5\text{cm}}$	°C	-0.08 ~ 0.91 (0.47)	97.2 (93.1)	2.8 (0)
$T_{s\_10\text{cm}}$	°C	-0.05 ~ 0.95 (0.47)	97.2 (93.1)	2.8 (0)
$T_{s\_20\text{cm}}$	°C	-0.06 ~ 0.98 (0.44)	97.2 (93.1)	2.8 (0)
$T_{s\_40\text{cm}}$	°C	-0.11 ~ 0.94 (0.40)	96.2 (80.8)	3.8(0)
$T_{s\_80\text{cm}}$	°C	-1.53 ~ 1.79 (0.14)	57.1 (20.9)	42.9 (7.7)
$T_{s\_160\text{cm}}$	°C	-1.43 ~ 1.57 (0.18)	60.4 (27.5)	39.6 (4)
$T_{s\_320\text{cm}}$	°C	-1.19 ~ 1.50 (0.17)	65.6 (31.1)	34.4 (5.6)

759

760

761

762

763

764

765

766

767

768

769

770



771 **Table 2.** Correlations between latitude, longitude, altitude and temperature trends on the Tibetan

772 Plateau.

Indices	Longitude	Latitude	Altitude
$T_{\text{air}}$	-0.10	0.19	0.35 <sup>b</sup>
$T_{s\_0\text{cm}}$	-0.11	0.23 <sup>b</sup>	0.31 <sup>b</sup>
$T_{s\_5\text{cm}}$	-0.005	0.05	0.16
$T_{s\_10\text{cm}}$	-0.04	0.07	0.24 <sup>a</sup>
$T_{s\_20\text{cm}}$	-0.13	0.01	0.36 <sup>b</sup>
$T_{s\_40\text{cm}}$	-0.19	-0.24	0.44 <sup>b</sup>

773 <sup>a</sup> Significant at the 0.05 level (t-test)

774 <sup>b</sup> Significant at the 0.01 level (t-test)

775

776

777

778

779

780

781

782

783

784

785

786

787

788

789

790

791



792 **Table 3.** Correlations between regionally averaged temperature indices and atmospheric circulation  
 793 indices over the Tibetan Plateau from 1981 to 2021.

Indices	$T_{\text{air}}$	$T_{s\_0\text{cm}}$	$T_{s\_5\text{cm}}$	$T_{s\_10\text{cm}}$	$T_{s\_20\text{cm}}$	$T_{s\_40\text{cm}}$
AMO	0.77 <sup>b</sup>	0.78 <sup>b</sup>	0.76 <sup>b</sup>	0.76 <sup>b</sup>	0.78 <sup>b</sup>	0.77 <sup>b</sup>
AO	-0.10	-0.05	-0.04	-0.02	-0.02	-0.04
NAO	-0.31 <sup>a</sup>	-0.31 <sup>a</sup>	-0.29	-0.27	-0.27	-0.28
PDO	-0.33 <sup>a</sup>	-0.36 <sup>a</sup>	-0.35 <sup>a</sup>	-0.34 <sup>a</sup>	-0.35 <sup>a</sup>	-0.40 <sup>b</sup>
MEI	-0.40 <sup>b</sup>	-0.37 <sup>a</sup>	-0.35 <sup>a</sup>	-0.34 <sup>a</sup>	-0.35 <sup>a</sup>	-0.40 <sup>a</sup>
Nino 3.4	-0.16	-0.10	-0.09	-0.08	-0.08	-0.14
WPI	0.04	-0.03	-0.04	-0.04	-0.03	0.01
SASMI	-0.20	-0.22	-0.27	-0.28	-0.25	-0.23
EASMI	-0.10	-0.07	-0.06	-0.06	-0.05	-0.06

794 <sup>a</sup> Significant at the 0.05 level (t-test)

795 <sup>b</sup> Significant at the 0.01 level (t-test)

796

797

798

799

800

801

802

803

804

805

806

807

808

809

810